UCRL-JC-133686
PREPRINT

Measurements of Deep Heating Generated by Ultra-Intense Laser-Plasma Interactions

J. A. Koch, S. P. Hatchett, M. H. Key,
R. W. Lee, D. Pennington,
R. B. Stephens, and M. Tabak

This paper was prepared for submittal to the
First International Conference on Inertial Fusion Sciences and Applications
Bordeaux, France
September 12-17, 1999

August 25, 1999

Lawrence
Livermore
National
Laboratory

This is a preprint of a paper intended for publication in a journal or proceedings. Since changes may be made before publication, this preprint is made available with the understanding that it will not be cited or reproduced without the permission of the author.

DISCLAIMER

This document was prepared as an account of work sponsored by an agency of the United States Government. Neither the United States Government nor the University of California nor any of their employees, makes any warranty, express or implied, or assumes any legal liability or responsibility for the accuracy, completeness, or usefulness of any information, apparatus, product, or process disclosed, or represents that its use would not infringe privately owned rights. Reference herein to any specific commercial product, process, or service by trade name, trademark, manufacturer, or otherwise, does not necessarily constitute or imply its endorsement, recommendation, or favoring by the United States Government or the University of California. The views and opinions of authors expressed herein do not necessarily state or reflect those of the United States Government or the University of California, and shall not be used for advertising or product endorsement purposes.

Measurements of Deep Heating Generated by Ultra-Intense Laser-Plasma Interactions

J. A. Koch, S. P. Hatchett, M. H. Key, R. W. Lee, D. Pennington,
R. B. Stephens*, M. Tabak

Lawrence Livermore National Laboratory
P.O. Box 808, L-481, Livermore CA, 94551
**General Atomics, San Diego CA 92186*

Abstract

We measure 300 eV thermal temperatures at near-solid densities by x-ray spectroscopy of tracer layers buried up to 30 μm inside CH slabs which are irradiated by a 0.5 kJ, 5 ps laser. X-ray imaging data suggest that collimated electron transport produces comparable temperatures as deep as 200 μm, and unexpectedly show the heated regions to be 50-120 μm-diameter rings. The data indicate that intense lasers can directionally heat solid matter to high temperatures over large distances; the results are relevant for fast-ignition inertial-confinement fusion and hot, dense plasma research.

Chirped pulse amplification (CPA) techniques[1] can provide laser irradiances exceeding $I = 10^{20}$ W/cm^2, and this enables experimental study of relativistic laser-plasma interactions. In this regime, electron quiver energies exceed the electron rest energy[1,2], and self-focusing[3,4], hole-boring[5], and critical-density absorption convert laser energy into an intense directed beam of relativistic electrons with a suprathermal temperature T_{hot} approximately proportional[6] to $\sqrt{I\lambda^2}$, where λ is the laser wavelength. These electrons can efficiently heat high-density matter. The fast-ignitor scheme[7] for inertial-confinement fusion[8] proposes to utilize this process to ignite pre-compressed thermonuclear fuel with MeV electrons produced by a ~ 10 ps, $I\lambda^2 \sim 10^{19}$ W μm^2/cm^2 laser pulse, but the physics of this scheme is still at an early stage of investigation[9]. The production of hot, dense matter is also of more general interest for strongly-coupled laboratory and astrophysical plasma physics.

Energy transport by relativistic electrons is complex, since strong electric and magnetic fields self-consistently modify their trajectories. Toroidal magnetic fields can shield target surfaces, resulting in a ring-pattern of energy deposition around a central hot-spot due to back-emitted electrons returning to the surface[10]. Space-charge electric fields can reduce electron penetration into dense targets[11], and can induce strong charge-return currents. Particle-in-cell simulations show that electron flow can filament at high densities[12], but more global modeling[13,14] and some experiments[15] indicate a beneficial net collimation effect due to the magnetic field generated by the current. This magnetic field may in turn be modified by conductivity discontinuities in a layered target[16].

All these processes affect the deep heating of solid matter by laser-generated electrons, and experimental data is required to guide research. Earlier experiments investigated thermal[17,18] and relativistic[19] electron heating at < 5 μm depths, but these depths did not exceed the laser focus diameter. Our experiments use x-ray imaging and spectroscopy of buried tracer layers to demonstrate strong heating up to 200 μm into solid targets, a depth ~ 25 times the laser focus diameter. The data support an emerging picture of magnetically-collimated relativistic electron transport and energy deposition while providing new questions for further research.

In our experiments, a λ=1.054 μm, 0.5 kJ laser[20], focused to an 8 μm-diameter spot with an f/3 parabolic mirror, achieved peak vacuum irradiances of 3×10^{19} W/cm^2 with 5 ps pulses. Some experiments were also performed using 20 ps pulses with proportionally reduced irradiances. The laser produces a 4 ns duration, ~ 1.5×10^{-5} energy-contrast amplified spontaneous emission (ASE) pedestal and a ~ 3×10^{-4} leakage pre-pulse 2 ns before the main pulse.

The targets were multilayers of two types. The first, 5 to 50 μm CH/0.5 μm Al or Au/100 μm CH, was diagnosed from the front (laser-side), while the second, 50 to 200 μm CH/0.5 μm Au/5 μm CH, was diagnosed from the rear in order to minimize attenuation of the metal-tracer x-ray emission by thick CH. The front CH layer was irradiated at 0° or 45° p-polarized, and each layer covered the full 1.5x1.5 mm^2 area of the targets.

Three diagnostics viewed the x-ray emission from the Al or Au tracer layers. The first was a pinhole camera, with a filtered array of 10 μm pinholes in a Ta substrate projecting images onto film or an x-ray charge-coupled device (CCD). The camera imaged the front or the back of the target, depending on the experiment, with a spatial resolution of ~ 10 μm for x-ray energies > 1.5 keV. The second diagnostic was a concave-spherical mica crystal spectrograph[21], which delivered a spectral resolution $\Delta E/E < 2.5\times10^{-3}$ onto an x-ray CCD. The third diagnostic was a convex-cylindrical potassiumhydrogen-phthalate (KAP) crystal spectrograph, which delivered a spectral resolution $\Delta E/E < 5\times10^{-3}$ onto a streak camera with a time resolution of 25-80 ps depending on the experiment. The spectrographs were operated on front-view Al-tracer experiments only.

Representative x-ray images are shown in Fig. 1. Front-view Al tracers 10-25 μm deep showed annular images with 70-120 μm inner diameters, typically containing several bright spots along the circumference and exhibiting a peak/center contrast ratio > 5; a front-view Au tracer 15 μm deep showed a similar 70 μm-diameter ring. Front-view Al tracers 30-50 μm deep showed ~ 50 μm regions of arc-like structure, possibly due to weaker signals which permitted only the brightest portions of the rings to be observed. Rear-view Au tracers 50-100 μm deep showed rings 50 μm in diameter. We also obtained a rear-view image from a Au tracer 200 μm deep, but the exposure was too weak to exhibit structure. Finally, front-view solid Au and Al targets typically showed bright sub-20-μm spots, in marked contrast to the other data. No clear correlations between ring diameter and tracer depth or material have been found, but ring emission appears to be a characteristic feature of the buried-tracer data, and the rings appears nearly circular in a plane normal to the laser axis even with a 45° p-polarized target orientation. We discuss this data in more detail shortly.

Spectroscopic data confirm that the rings are emitted from the buried metal tracers, since Al tracer targets show emission lines from highly ionized Al (Fig. 2). The integrated exposures of the spectra and the pinhole images are strongly correlated, indicating that the spectra are emitted from the bright regions of the images. In addition, time-resolved spectra indicate that all keV x-ray emission takes place within a ~ 70 ps time window.

We use the spectrally-integrated Al XII line ratio ($2p^2\ {}^1D_2$-$1s2p\ {}^1P_1$)/($1s3p$-$1s^2$), He-J/He-β, as a bulk electron temperature (T_e) diagnostic by fitting the measured ratios to simulated local thermodynamic equilibrium (LTE) optically-thin spectra from the code TOTAL[22]. This ratio is independent of electron density N_e and instrument resolution, and based on scaling from other data[23] it is expected to be valid despite a strong suprathermal electron flux when $N_e > 2 \times 10^{22}$ cm^{-3}. This condition is satisfied in our experiments, and the high density also supports the use of LTE kinetics. The maximum optical depth for the He-J and He-β lines is predicted to be 0.6, justifying the optically-thin approximation in the simulations. The He-J/He-β ratio is expected to be a more reliable measure of T_e than the He-β/Ly-β ratio[23,21], and isoelectronic lines are more likely to be emitted from the same spatial regions. For a density diagnostic, we fit the blue-wing half-width of the He-β to simulated spectra from the code FLY[24]. These simulations used steady-state kinetics with a constant 2.7 g/cm^3 * 0.5 μm areal density (ρR) at the T_e values inferred from the TOTAL simulations. A representative spectrum with a TOTAL fit is shown in Fig. 2(a). All data were corrected for energy-dependent filter transmission, crystal peak reflectivity, and detector efficiency, and the simulated spectra were smoothed by the measured spectral resolution prior to comparison with the data.

Self-consistent time-integrated T_e and mass density (ρ) data are shown in Fig. 3. For Al at 5-30 μm depths, we find T_e = 270-340 eV and ρ = 0.25-0.95 g/cm^3, corresponding to N_e = 0.7-2.0x10^{23} cm^{-3}. We do not observe any systematic dependence of T_e or ρ upon tracer depth, suggesting nearly isothermal heating at constant density. Al spectra from 50 μm depths were also observed, but the data were too weak for analysis. Sub-solid Al densities are expected by pressure-balance arguments ($(\overline{Z}+1)\rho / A$ is constant), and the

Al layer will expand to ~ 1.2 g/cm^3 when surrounded by isothermal solid-ρ CH. The Al density will further decrease if the surrounding CH is cooler.

The Al emission persists long after the laser pulse, with a full-width at half-maximum duration of ~ 70 ps. This supports the conclusion that the Al emission is thermal, and that the Al cools gradually by conduction. The He-β is not observed to narrow in time, indicating near-constant density over the emission duration, but it appears 20-50 ps later than the Ly-α and the He-J. Time-varying He-J/He-β ratios suggest peak temperatures of ~ 450 eV, and the He-β/Ly-β ratio also indicates T_e = 450-550 eV, though this ratio is probably less reliable as noted above. We also observe the appearance of satellites on the red wing of the Ly-α at greater depths (Fig. 4). These satellite features peak early, and are possibly emitted from hole-states populated by inner-shell collisional ionization and excitation[25]. Similar features dominate spectra obtained with fast-rising CPA laser irradiation of solid Al and Mg targets[26], and the appearance of these satellites is consistent with heating at near-solid density caused by suprathermal electrons.

We do not have spectra for tracer depths > 50 μm, but we infer comparable temperatures at depths as great as 200 μm. The exposures of the Al-tracer pinhole images will scale strongly[24] with T_e below 400 eV, where the emission is dominated by the optically-thick He-α in the Wien region of the thermal spectrum. Observable images were obtained with identical filtering on all the Al experiments, supporting the conclusion of nearly depth-independent heating; similar conclusions hold for the (much higher ρR) Au-tracer data from depths as great as 200 μm. We note that it is energetically feasible to fully ionize a 50 μm-diameter, 200 μm-deep column of 1 g/cm^3 CH and heat it to 300 eV, since this would require only ~ 15 J.

Taken together, the data indicate that laser-generated relativistic electrons can heat solid matter to 200-300 eV temperatures at depths as great as 200 μm into CH targets. This depth is ~ 25 times the laser focal spot diameter, and the similarity of the x-ray images from different depths and the nearly depth-independent T_e and ρ data support a picture of magnetically-collimated relativistic electron transport[13,14]. However, the observation of annular x-ray images with diameters much greater than the laser focal spot diameter was unexpected. Lack of measurable emission from the centers of the rings could be attributed to a much less-dense center, to a strong overionization of the center, or to a cooler center. The first two mechanisms may be rejected as inconsistent with our total data set and supporting simulations.

Regarding the first mechanism, we performed 2-D hydrodynamics simulations[27] of the interaction of the ~ 150 mJ ASE and pre-pulse with the buried-Al targets to predict the on-axis local Al electron density at t = 0 as a function of initial layer depth. This density is 1.5×10^{22} cm^{-3} for an initial depth of 15 μm, potentially resulting[24] in a factor of ~ 5 reduction in per-atom Al emissivity at constant T_e = 300 eV; however, layers at initial depths > 50 μm are totally unaffected by the ASE and pre-pulse. During the 5 ps main laser pulse, we estimate a peak ponderomotive pressure I/c ≈ 17 Gbar and a front speed $\sqrt{P/\rho}$ ≈ 1.3×10^{8} cm/s, resulting in a hole-boring depth of ~ 6 μm; this agrees with other estimates[6], and is too small to account for the rings. Later ablation of the target would proceed at ion sound speeds of ~ 2×10^{7} cm/s, too slow to reach the deeply buried tracers in ~ 70 ps.

Regarding the second mechanism, overionization of the central portions of the tracer layers would require multi-keV temperatures which were not seen in similar solid-target experiments measuring thermal D_2

neutrons[28]. Furthermore, we see no evidence for subsequent cooling and recombination emission, and the lack of observed central hot-spots in the time-integrated images of the deeply-buried tracers appears to be inconsistent with this mechanism. Finally, the sharp intensity gradient on the inner edge of the rings appears to be inconsistent with both mechanisms.

We conclude that the central portions of the rings do not emit because they are cooler ($T_e < 230$ eV) while remaining at near-solid densities. As noted above, our data generally support a picture of magnetically-collimated relativistic electron flow described by Davies *et al.* [13,14]. However, their simulations predict currents which are collimated within a ~ 30 μm-diameter area, and do not predict the annular heating which characterizes our data. We therefore consider their simulations in more detail, using the specific parameters of ref. [14].

Davies *et al.* assume that a ~ 20 J laser focused onto a target generates a time- and space-varying electron source with a Boltzmann energy distribution, $\exp(-\varepsilon/T_{hot}(r,t))$. They assume $I \propto \exp(-r^2/R^2 - t^2/\tau^2)$, with $\tau = 0.5$ ps and $R = 6$ μm; they also assume a constant energy conversion efficiency $f_{abs} = 0.2$, and assume $T_{hot}(r,t) \propto I(r,t)^{1/3}$. Electrons enter a CD_2 target within a 15° half-angle cone, and their trajectories are determined self-consistently up to $t = 4\tau$; local heating is caused by forward- and return-current energy losses. They do not treat laser-plasma interactions or electron flow instabilities, and they require $T_{hot} >> T_e$ and $N_{hot} << N_e$, the latter assumption potentially becoming questionable above 10^{19} W/cm^2 intensity[13]. They note that target conductivity strongly affects electron transport, and that increased local conductivity due to heating is an important factor in channel formation.

Comparisons between these simulations and our experiments suggest several areas for further study. First, relativistic laser propagation through under-dense plasma has been investigated separately and shown to strongly affect laser intensity profiles at critical density[3]. A consistent treatment of laser-generated electron transport through solid targets, including laser-plasma interactions in plasma created by realistic levels of laser ASE and pre-pulse, would thus be valuable. Second, conductivity discontinuities (i.e. metal tracers) could affect energy deposition in the vicinity of the tracers, as has been noted earlier[16], and these are not treated in the simulations. Third, the return-current electron drift velocity in our experiments exceeds the ion-acoustic velocity, potentially limiting current densities due to ion-acoustic turbulence and increasing the magnetically-collimated areas[29] beyond those calculated by Davies *et al.* Fourth, the x-ray emission duration in our experiments is much longer than the laser pulse duration, and plasma evolution over ~ 100 ps timescales is not treated in the simulations. Fifth, the global approximations $T_{hot} \propto I^{1/3}$ and f_{abs} = constant are not strictly valid, and different assumptions could result in qualitatively different behavior, possibly further modified by laser-plasma interactions. To illustrate the last point, if T_{hot} locally tracks the laser intensity profile and scales as I^{α}, if $d\varepsilon/dx \propto 1/\varepsilon_0^{\beta}$, and if $f_{abs} \propto I^{\gamma}$, then the volumetric energy absorption from forward-traveling electrons at shallow depths scales as $I^{((1+\gamma)-\alpha(1+\beta))}$, producing a local *minimum* where the intensity is largest if the exponent is negative (reasonable estimates $\alpha = 0.5$, $\beta = 1$ and $\gamma = 0$ predict a null exponent). Finally, additional experiments would be valuable, including pre-pulse and intensity parameter scans, space-resolved spectroscopy, and high-energy Kα imaging[30].

In summary, our data provide evidence for quasi-collimated relativistic electron transport deep into CH targets, resulting in > 70 ps-duration heating to T_e ~ 300 eV at near-solid densities for depths up to 200 μm. The annular heating patterns we observe are not yet understood, and we suggest several paths for further research in this area. The results also demonstrate the potential of intense laser beams to efficiently produce hot, dense matter. We gratefully acknowledge S. Alvarez, J. Bower, C. Brown, E. M. Campbell, R. Costa, A. Faenov, B. Hammel, J. Kilkenny, O. Landen, A. MacKinnon, M. Moran, A. Offenberger, M. Perry, T. Pikuz, R. Robinson, C. Sangster, R. Snavely, M. Tsukamoto, R. Wallace, S. Wilks, and K. Yasuike for their contributions and support. This work was performed under the auspices of the U.S. Department of Energy by the Lawrence Livermore National Laboratory under contract No. W-7405-ENG-48, with the additional corporate support of General Atomics.

References

[1]M. D. Perry and G. Mourou, Science **264**, 917 (1994).

[2]P. Gibbon and E. Förster, Plasma Phys. Control. Fusion **38**, 769 (1996).

[3]A. Pukhov and J. Meyer-ter-Vehn, Phys. Rev. Lett. **76**, 3975 (1996).

[4]M. Borghesi *et al.*, Phys. Rev. Lett. **78**, 879 (1997).

[5]R. Kodama *et al.*, Phys. Rev. Lett. **77**, 4906 (1996).

[6]S. C. Wilks, Phys. Fluids B **5**, 2603 (1993).

[7]M. Tabak *et al.*, Phys. Plasmas **1**, 1626 (1994).

[8]J. D. Lindl, Phys. Plasmas **2**, 3933 (1995).

[9]M. H. Key *et al.*, Phys. Plasmas **5**, 1966 (1998), and references therein.

[10]M. D. J. Burgess *et al.*, Phys. Fluids **28**, 2286 (1985).

[11]A. R. Bell *et al.*, Plasma Phys. Control. Fusion **39**, 653 (1997).

[12]B. F. Lasinski *et al.*, Phys. Plasmas **6**, 2041 (1999).

[13]J. R. Davies *et al.*, Phys. Rev. E **56**, 7193 (1997).

[14]J. R. Davies *et al.*, Phys. Rev. E **59**, 6032 (1999).

[15]M. Tatarakis *et al.*, Phys. Rev. Lett. **81**, 999 (1998).

[16]A. R. Bell *et al.*, Phys. Rev. E **58**, 2471 (1998).

[17]G. J. Tallents *et al.*, Phys. Rev. A **40**, 2857 (1989).

[18]G. Guethlein *et al.*, Phys. Rev. Lett. **77**, 1055 (1996).

[19]J. A. Koch *et al.*, Lasers and Particle Beams **16**, 225 (1998).

[20]M. D. Perry *et al.*, Opt. Lett. **24**, 160 (1999).

[21]J. A. Koch *et al.*, Rev. Sci. Instrum. **70**, 525 (1999).

[22]B. Talin *et al.*, J. Quant. Spectrosc. Rad. Transfer **58**, 953 (1997), and references therein.

[23]F. B. Rosmej, J. Phys. B **28**, L747 (1995).

[24]R. W. Lee and J. T Larsen, J. Quant. Spectrosc. Rad. Transfer **56**, 535 (1996).

[25]F. B. Rosmej *et al.*, J. Phys. B **29**, L299 (1996).

[26] F. B. Rosmej *et al.*, JETP Lett. **65**, 708 (1997).

[27] LASNEX; see G.B. Zimmerman and W.L. Kruer, Com. Plasma Phys. Controlled Fusion **2**, 51 (1975).

[28] C. Sangster, unpublished LLNL data.

[29] J.-P. Matte, personal communication.

[30] J. A. Koch *et al.*, Appl. Opt. **37**, 1784 (1998).

Figure Captions

Figure 1: X-ray pinhole images of an Al tracer 15 μm deep (a), a Au tracer 50 μm deep (b), a Au tracer 100 μm deep (c), and solid Au (d). In each case, ~ 20 individual pinhole images from the same experiment were averaged to improve signal-to-noise, and the results were corrected for a normal-incidence viewing angle.

Figure 2: Mica spectrograph data (b) and KAP spectrograph data (c) from an Al layer 10 μm deep. The conical shape in (b) results from the focusing geometry[21]. A fit to the mica data is shown in (a) along with the inferred T_e and ρ.

Figure 3: Spectroscopic T_e and ρ data from the buried Al experiments. Uncertainties are estimated from known sources of random and systematic errors, and data from both spectrographs are included.

Figure 4: Comparison of Al spectra from 10 and 30 μm depths. The temperatures inferred from the He-J/He-β ratios are the same, but the deeper spectrum contains numerous satellite features which may be caused by suprathermal electrons.

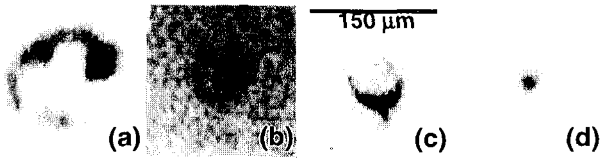
150 µm
(a)
(b)
(c)
(d)

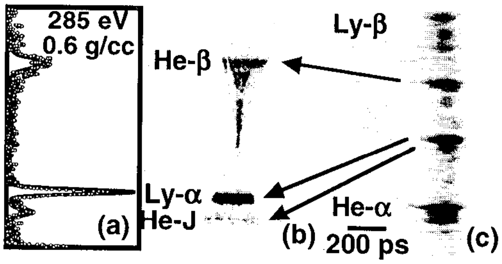
285 eV
0.6 g/cc
He-β
Ly-β
Ly-α
He-J
He-α
200 ps
(a)
(b)
(c)

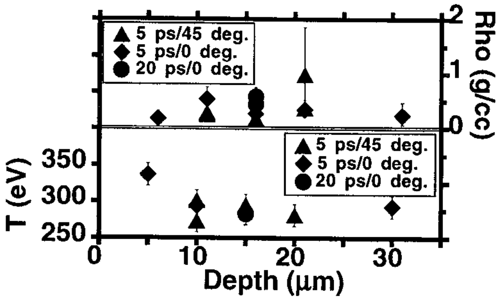

▲ 5 ps/45 deg.
◆ 5 ps/0 deg.
● 20 ps/0 deg.
Rho (g/cc)
2
1
0
▲ 5 ps/45 deg.
◆ 5 ps/0 deg.
● 20 ps/0 deg.
T (eV)
350
300
250
0
10
20
30
Depth (μm)

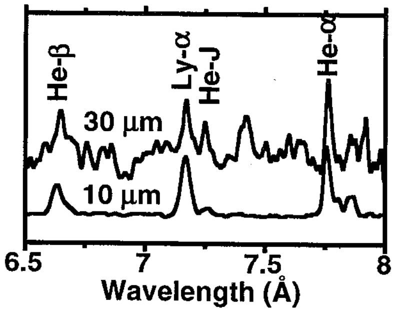
He-β
Ly-α
He-J
He-α
30 μm
10 μm
6.5
7
7.5
8
Wavelength (Å)